Coordination Chemistry Reviews 254 (2010) 2505–2518

Contents lists available at ScienceDirect

Coordination Chemistry Reviews

journal homepage: www.elsevier.com/locate/ccr

Review

Understanding excited-state structure in metal polypyridyl complexes using resonance Raman excitation profiles, time-resolved resonance Raman spectroscopy and density functional theory

Raphael Horvath, Keith C. Gordon*

MacDiarmid Institute for Advanced Materials and Nanotechnology, Chemistry Department, University of Otago, Union Place, Dunedin, Otago 9010, New Zealand

Contents

ARTICLE INFO

Article history:
Received 29 September 2009
Accepted 13 November 2009
Available online 22 November 2009

Keywords:
Metal polypyridyl
Raman
Wavepacket analysis
Density functional theory

ABSTRACT

This article discusses the use of Raman spectroscopy, in concert with density functional theory, as a strategy for understanding excited-state structure in metal polypyridyl complexes. The first sections of the article discuss how one can use resonance Raman spectra of the ground-state molecule to understand the resonant Franck-Condon excited state. The theories behind these analyses are based on the sum-over-states and time-dependent approaches; a brief introduction to each of these methods is given. The use of density functional theory and its use in the determination of normal modes of vibration and infrared and Raman band intensities are discussed, with reference to a number of recent papers. The application of these methods is illustrated through the analysis of a number of selected examples which exemplify the strategies used to extract data from probing the Franck-Condon region. These data include the displacements of the resonant excited state with respect to the electronic ground state, the reorganisation energies associated with photoexcitation, bond length changes with excitation and other electronic parameters. The use, and limitations, of these methods are discussed. The direct calculation of resonance Raman band intensities is introduced. The direct measurement of excited-state vibrational spectra through time-resolved methods is discussed in the latter section of the article; with particular regard to the use of transient resonance Raman and time-resolved resonance Raman techniques to probe structural changes in metal polypyridyl complexes.

1. Introduction

Many metal complexes incorporating polypyridyl ligands offer interesting properties with strong transitions across the entire visible region. These transitions are of considerable interest both from a fundamental perspective and because of their utility in a variety of applications, including solar energy systems [1–8]. For complexes with d^6 metals, such as ruthenium(II), rhenium(I), and the d^{10} metal copper(I), the lowest energy transitions are metal-to-ligand charge-transfer (MLCT) in nature. As such they offer interesting systems to investigate electron-transfer phenomena as the metal is formally oxidised and the ligand reduced upon photoexcitation.

* Corresponding author.
E-mail address: kgordon@chemistry.otago.ac.nz (K.C. Gordon).

0010-8545/$ – see front matter © 2009 Elsevier B.V. All rights reserved.
doi:10.1016/j.ccr.2009.11.015

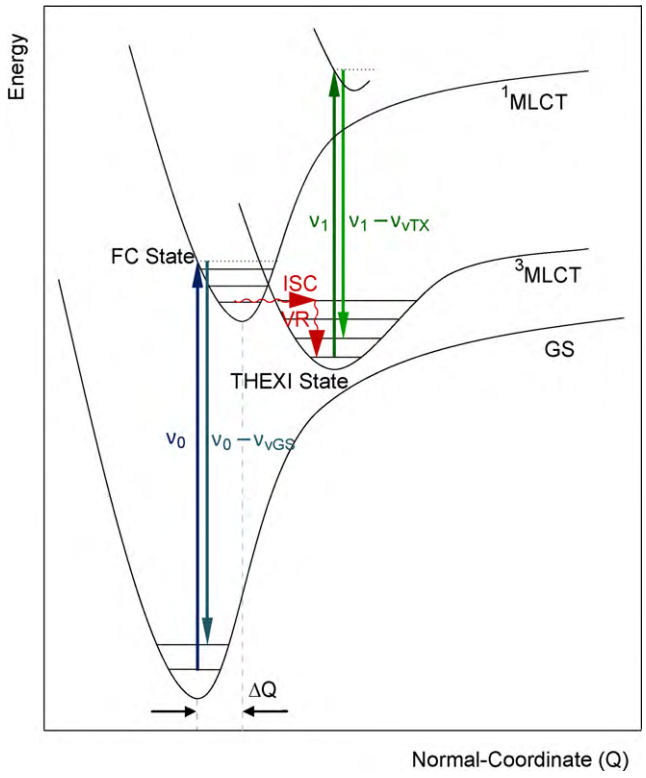

Fig. 1. Some of the photophysical processes probed by Raman spectroscopic techniques. Resonance Raman (using a single continuous-wave laser, ν_0), can probe the Frank-Condon state while time-resolved resonance Raman (using two pulse-lasers, ν_0 and ν_1) probes the longer-lived THEXI state.

Fig. 1 summarises some of the aspects of photoexcitation of these complexes and how Raman spectroscopy can shed light on the species involved. Resonance Raman spectroscopy is able to probe the Franck-Condon (FC) state; that is, the vibrationally hot ^{1}MLCT state. This state is very short-lived (and thus structurally similar to the ground state) and one is able to extract ultrafast dynamics, such as the change in equilibrium bond lengths upon electronic excitation, from the analyses of resonance Raman spectra.

Population of the ^{1}MLCT state is generally followed by intersystem crossing and vibrational relaxation (ISC and VR, shown as waved lines) on a picosecond timescale to a low-lying ^{3}MLCT state, also known as the thermally equilibrated excited (THEXI) state [9]. This state can be important in the design of functional devices as for MLCT-type transitions it represents a relatively long-lived and thus accessible charge-separated state, in which the metal and ligand are essentially oxidised and reduced, respectively. It can be probed by time-resolved resonance Raman (TR^3) spectroscopy , which utilises two laser pulses to successively populate and probe the state in question [10,11]. The state dynamics can be monitored by adjusting the time-delay between the laser pulses whereas independent adjustment of the laser energies allows for efficient population of the state in question while maintaining resonance with the one above it. A variation of TR^3 is transient resonance Raman (TR^2) spectroscopy, in which only a single laser pulse is used to both generate and probe the excited state [12]. Due to the long-lived nature of the THEXI state in many compounds, TR^2 is inherently biased to the observation of this state, making it a popular alternative to TR^3 at a lower complexity of experimental setup.

Density functional theory (DFT) computational methods have become widely used in the last 10 years and continue to be developed to yield faster and more accurate calculations [13]. With DFT it has become possible to step beyond the empirical analysis of vibrational spectra; one can now predict structure, electronics and energetics of the ground and excited states and calculate vibrational spectra that directly relate spectral peaks to normal modes of vibrations, which has been well demonstrated using infrared spectroscopy. The success of DFT in predicting vibrational spectra is not always guaranteed and there are a variety of tests that may be used to validate the efficacy of calculations. In this review we discuss, with a series of selected examples, how one can use Raman spectroscopy in concert with computational chemistry to understand the structures and dynamics of coordination compounds in their ground, Franck-Condon electronically excited, and thermally relaxed excited states (Fig. 1). The probing of each of these types of states is the domain of resonance Raman and transient or time-resolved vibrational spectroscopy [13–17].

2. The FC state—resonance Raman scattering

The FC state (Fig. 1) may be probed through analysis of the resonance Raman scattering. The intensity of Raman scattering from vibrational states $i \rightarrow f$, (I_{if}) which differ in frequency by ν_{if} is given by [18]:

$$I_{if} = kI_0(\nu_0 + \nu_{if})^4 \sum_{\rho\sigma} |(\alpha_{\rho\sigma})_{if}|^2 \quad (1)$$

where I_0 is the intensity of incident radiation of frequency ν_0 and k contains universal constants. At the centre of Eq. (1) is the $\rho\sigma$th component of the transition polarisability tensor $(\alpha_{\rho\sigma})_{fi}$.

It is found that if the excitation laser wavelength (λ_{ex}) is coincident with an electronic transition of the molecule of interest then the Raman scattering is enhanced by up to six orders of magnitude; this enhancement is not random and is strongly mode-dependent [19]. For example, consider the normal Raman and resonance Raman spectra for the metal complex $Re(CO)_3Cl(biq)$, where biq = 2,2′-biquinoline, shown in Fig. 2. In the non-resonant spectrum the intensities of the bands are a consequence of the polarisability derivative for each normal mode. The biquinoline is a large π system, giving it several normal modes that are easily polarised and thus strong bands; in contrast the CO ligands show weaker Raman bands. However when the laser is tuned to 457.9 nm, which is in resonance with the MLCT transition of this compound, the spectrum is dramatically different; the biquinoline modes at 1380 and 1598 cm^{-1} do not show strong enhancement—in fact the spectrum is dominated by the in-phase stretch of the facial CO ligands at 2022 cm^{-1}. The reason for this enhancement is that this normal mode, in which the CO ligands stretch and compress in phase, is one of the normal coordinates that shows distinct structural distortion on going from the ground to the resonant excited state (Fig. 1) [20,21]. This relationship between resonance Raman enhancements and ground- to excited-state structural displacements was first enunciated by Hirakawa and Tsuboi [19] and subsequently developed by others [22]. Normal-coordinate displacements between ground- and excited-state geometry minima will be referred to as Δ, given in dimensionless normal-coordinates Q.

A theoretical approach that describes Raman scattering cross-sections based on a two-photon process involving the pure vibrational wavefunctions of the initial, final and virtual vibronic states $|\nu^I\rangle$, $|\nu^F\rangle$ and $|\nu^V\rangle$, respectively, has been derived by Albrecht [18]. A-term scattering is most commonly observed and is given by:

$$(\alpha_{\rho\sigma})^A = [\mu_\rho^0][\mu_\sigma^0] \sum_V \frac{\langle \nu^F|\nu^V\rangle\langle\nu^V|\nu^I\rangle}{E_V - E_\ell - i\Gamma_V} \quad (2)$$

Here the sum is over vibronic states V, with energies E_V, and E_ℓ is the energy of the incident radiation. Γ_V is the homogeneous linewidth of V, related to the lifetime of this state, and $[\mu_\rho^0]$ and

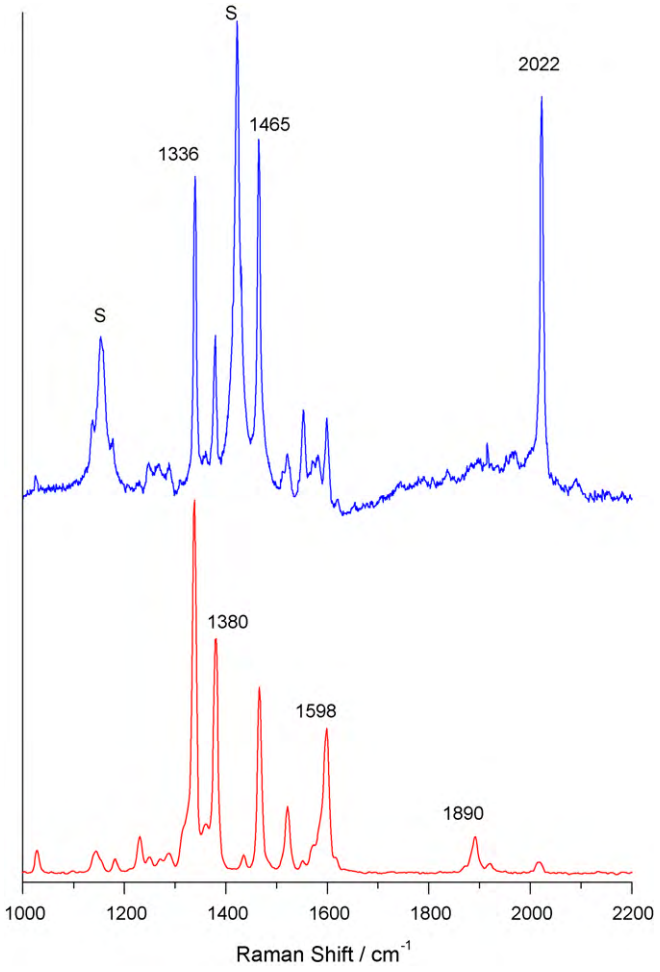

Fig. 2. Lower spectrum: normal Raman spectrum (λ_{exc} = 1064 nm) of a solid sample of Re(biq)$(CO)_3$Cl (biq = 2,2′-biquinoline). Upper spectrum: resonance Raman spectrum (λ_{exc} = 457.9 nm) of Re(biq)$(CO)_3$Cl (3 mM) in CH_2Cl_2. S denotes solvent bands.

$[\mu_\sigma^0]$ are the pure electronic transition moments for $|\nu^F\rangle \rightarrow |\nu^V\rangle$ and $|\nu^V\rangle \rightarrow |\nu^I\rangle$, respectively.

The sum-over-states methods describe in a physically appealing way a method of calculating resonance Raman intensities—but it can be difficult to implement; a different approach to this problem was introduced by Heller and co-workers [23,24] and applied by Myers [25,26]. The time-dependent theory involves excitation and subsequent propagation of a wavepacket on the excited-state surface. The appeal of this method is that if one has a good model of the FC surface then the absorption spectrum and Raman cross-sections may be evaluated through the time evolution of the overlap of the prepared wavepacket with the final state [24,26–30]. This may be contrasted by the sum-over-states model, which ipso facto requires an understanding of all the electronic states that contribute to the resonance effect.

At the heart of this method is the dynamic behaviour of the wavepacket created by the incident photon, $|i(t)\rangle$ (see Fig. 3). The Raman cross-section is related to the dynamic behaviour of this wavepacket relative to the final state $|f\rangle$. For the absorption process the overlap of the evolving $|i(t)\rangle$ wavepacket with the initial state $|i\rangle$ is key. The application of a half (for Raman) or full Fourier transform projects the time dynamic behaviour into wavenumber space and gives the resonance Raman excitation profile or absorption spectra, respectively. Clearly the degree to which the ground and excited electronic states differ, Δ, has a profound effect on the wavepacket dynamics and thus on absorption and resonance Raman spectra.

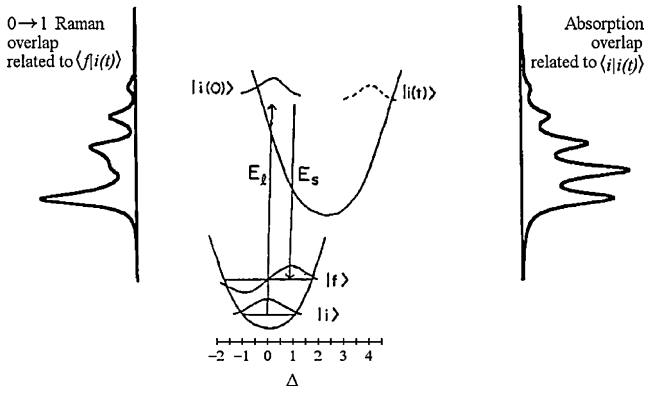

Fig. 3. Pictorial representation of the time-dependent approach to absorption and resonance Raman. The wavepacket $|i(t)\rangle$ propagates according to the excited-state Hamiltonian. The insets show the overlap with $|i(0)\rangle$ and $|f\rangle$ for absorption and resonance Raman, respectively. Details of relationships are given in Refs. [23–26]. Adapted with permission from Ref. [26].

The full time-dependent expression can be found in Refs [23,26]. Important to our discussion is the phenomenological decay constant, or dephasing term, Γ. This has a damping effect on the propagation of the wavepacket and thus influences the lifetime. For reasonably large molecules with a high number of degrees of freedom, this term is high [23]. This is because a larger number of dimensional coordinates have to return to the FC position along all $3N-6$ dimensions of normal-coordinate freedom simultaneously to give good overlap with the final state (where N is the number of atoms). As more time elapses, the likelihood of such an event becomes smaller, thus effectively the time-frame for the scattering event decreases. This is also known as a short time-limit case, where the wavepacket essentially only samples the gradient of the Franck-Condon state [31]. Furthermore Δ is generally small for larger molecules as modes tend to be spread out over a larger number of atoms. Evidence for this can be seen in the lack of structure in their absorption spectra. This implies the harmonic approximation for the excited state will give good results when the gradient of the FC state is used to interpret the resonance Raman excitation profiles in terms of Δ.

While these factors mean the time-dependent approach is computationally advantageous for large systems, it should be noted that the computational complexity of the sum-over-states method can be similar if one state is dominant. The first application of the time-dependent theory, carried out by Myers et al. [32] on the excited-state structure of isoprene and hexatriene, also provided a comparison to the sum-over-states method. It was found that for systems of moderate to high complexity the sum-over-states method was disadvantaged in terms of computational time, while giving equivalent results. Virtually all computed Raman profiles since then have utilised the time-dependent approach.

Using the sum-over-states or wavepacket analysis it is possible, in principle, to derive a number of useful parameters concerning the resonant excited state through analysis of pre-resonance or resonance Raman data or by fitting the resonance Raman excitation profiles, the differential Raman cross-sections (Raman band intensities) with respect to the excitation wavelength. These parameters include: (1) the dimensionless displacement (Δ) of the normal modes of vibration (Fig. 1); (2) the mode-dependent reorganisation energies (λ_ν) (*vide infra*) and (3) the dephasing time of the electronic transition (Γ, Eq. (2) and Ref. [26]). The methods by which these parameters may be evaluated and the assumptions made in the determination are discussed in the succeeding sections. However for many of the fitting and parameter evaluations to be valid the resonance Raman spectra must be measured in such a fashion that the differential Raman cross-section for the band of interest is

accurately established. This needs to be conducted with some care; the observed intensities are dependent on a number of factors such as excitation wavelength, absorption properties of the sample and bias within the detector and spectrograph.

Differential Raman cross-sections are obtained by comparison of the peak areas with reported differential Raman cross-sections of the solvent; to reduce errors in the measurement it is important that the concentration of the sample is chosen so Raman peaks are of similar intensity. This often requires a degree of trial and error; however, $\sim 10^{-3}$ mol L^{-1} is a good starting point. Accurate knowledge of this concentration is required. Baseline-correction is necessary to remove fluorescence and other effects adding to the background of a spectrum and to achieve accurate and consistent peak-integration. In our experiments [33] the integrated band intensities are obtained using the peak fitting module in Origin Pro 7.5. Solute differential Raman cross-sections were obtained relative to solvent cross-sections by:

$$\left(\frac{d\sigma_R}{d\Omega}\right)_u = \frac{I_u}{I_v}\frac{c_v}{c_u}\left(\frac{d\sigma_R}{d\Omega}\right)_v \quad (3)$$

in which $\left(d\sigma_R/d\Omega\right)_u$ is the differential Raman cross-section of the solute band of interest, I_u and I_v are the observed (fully corrected) intensities for the solute and solvent, respectively, c_u and c_v are the concentrations of solute and solvent and $\left(d\sigma_R/d\Omega\right)_v$ is the differential Raman cross-section of a solvent band. A number of these are reported for common solvents such as dichloromethane [33,34], chloroform [35], methanol [34] and DMSO [36].

Due to the high laser fluxes often used in Raman measurements, photodegradation of the sample can occur and should be assessed. This is most easily done by acquiring the absorption spectra before and after the Raman experiment. Thoroughly degassing the sample with an inert gas can prevent degradation but can cause evaporation and thus a change in concentration if a volatile solvent is used.

The fitting programs for wavepacket analysis of resonance Raman excitation profiles and absorption spectra have been developed, in large part by the Myers-Kelley group [37]. The procedure involves the iteration of parameters that include: (1) vibrational mode displacements (Δ), typically up to 30 modes may be considered; (2) the zero, zero point energy gaps between the ground and resonant electronic transition or transitions (E_{00}); (3) the transition dipole length for the electronic transition(s) (μ); (4) the homogeneous broadening of the electronic transition(s) (Γ_0) and (5) the inhomogeneous broadening (Γ_s).

Generally the derived parameters from these fits may be compared to the observed electronic absorption spectrum and the resonance Raman spectra. This is exemplified in a study on $[Ru(CN)_4ppb]^{2-}$ (ppb = dipyrido[2,3-a:3′,2′-c]phenazine) [38]. The derived values for Δ^2 and other parameters were applied to the time-dependent expressions of the absorption cross-section and Raman scattering to simulate the absorption spectrum (Fig. 4) and the resonance Raman spectrum (Fig. 5), respectively; the goodness of the respective fits is an additional test of the robustness of the analysis.

3. Quantifying the normal coordinate and calculated Raman intensities

The vexing question as to the nature of normal modes in complex molecules has been a challenge to spectroscopists as they try to understand larger more complex molecules. The problem is one of understanding the forces that hold the molecule together [39]. It is possible to establish this for metal polypyridyl complexes using Urey-Bradley force fields and careful selective and per-deuteration and other isotopic substitution of the ligands. The normal modes

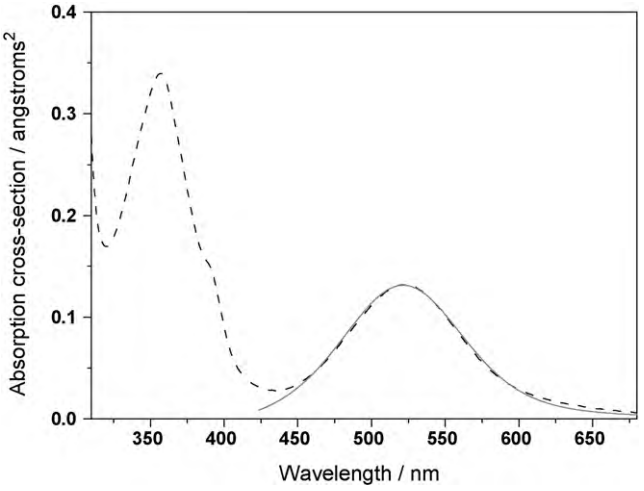

Fig. 4. Comparison of the simulated absorption spectrum (gray line) derived from wavepacket analysis to the experimental data (dashed line) for $[Ru(CN)_4ppb]^{2-}$ in water (adapted from Ref. [38]).

of vibration for $[Ru(bpy)_3]^{2+}$ (bpy = 2,2′-bipyridine) and its ^{3}MLCT state were reported by Strommen et al. [40] in which they examined a number of ^{2}D and ^{15}N isotopically labelled analogues of the complex. In both ground- and excited-state spectra the labelled compounds show significant decreases in vibrational frequencies owing to the increased reduced masses. This allows for normal-coordinate calculations (NCA), giving vibrational assignments, a map of force-constants and potential energy distribution in both GS and the ^{3}MLCT state. A problem with this approach is that a large

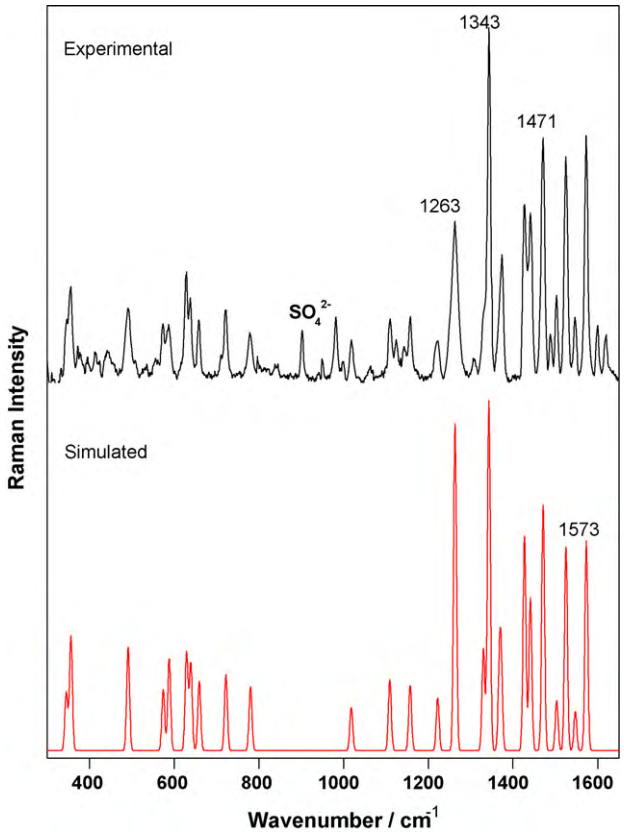

Fig. 5. Comparison of the simulated resonance Raman spectrum (lower trace) with the experimental data (upper trace) for $[Ru(CN)_4ppb]^{2-}$ in water. Note the sulfate internal standard band in the experimental spectrum (adapted from Ref. [38]).

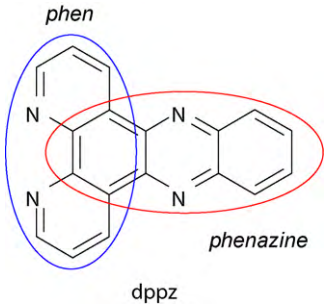

Fig. 6. Structure of dipyridophenazine with the phenanthroline (phen) and phenazine portions.

number of experimental frequencies, and thus isotopically labelled molecules, are required to make the NCA meaningful. The advent of computational chemistry has dramatically altered the way in which vibrational spectra are analysed for metal complexes. For example detailed studies of selective and perdeuerated dipyridophenazine (dppz) and rhenium complexes thereof [41,42], with the aid of DFT calculations, allowed a detailed assignment of the vibrational normal modes of dppz. Distinct normal modes were found for localised phenazine (phz) and phenanthroline (phen) ring-sections of the framework, corresponding to activity in the respective part of the ligand (see Fig. 6). From this analysis it appears that the MLCT transition of these rhenium complexes terminates on a phen-based π^* acceptor orbital. For an extensive review on dppz as a light-switch see Browne and McGarvey [43].

As quantum calculations become faster and more widely available, more emphasis is placed on them rather than somewhat more laborious studies such as isotopic labelling. While this enables studies to be carried out much more efficiently, an important question becomes—how well can one trust the calculated data? There are several strategies that may be used to gain confidence in the calculation with regard to the real system: (1) the level of theory and basis sets used may be increased in a systematic way and the properties of interest analysed to see if the calculation is converging; (2) the calculated structure may be compared to an observable property such as geometry or vibrational spectrum. Strategy (1) is an extremely good method of testing the calculations—unfortunately it is not always possible when examining transition-metal complexes and thus strategy (2) becomes relevant. The most obvious implementation of this is a comparison between the calculated geometry and that measured by X-ray crystallography. However, relying on X-ray data as the only confirmation of the integrity of the calculated structure is rarely an effective test. If DFT is to be used in understanding geometric distortions with regard to the resonant excited state relative to the ground electronic state then the vibrational modes need to be well modelled—the most obvious way to gauge this is to examine the differences between real experimental vibrational data and those calculated.

If one is to use resonance Raman spectroscopy to analyse the structure of the resonant excited state then the vibrational spectrum is required and indeed becomes a rather useful test of the calculation.

The key test is correlating the calculated frequencies to the experimental data [44,45]. This has been used in a study of the spectroscopy and DFT modelling of $[Cu(phen)(PPh_3)_2]^+$ [46]. The comparison between experimental and calculated vibration data was parameterised by the frequency mean absolute deviation (MAD) [21,47–49] for the most intense bands (generally those of >20% the most intense feature). In general it is found that if the MAD is <10 cm^{-1} then other electronic parameters correlate well [21,46,47,50,51]. Some care is required in dealing with intensity outputs from programmes such as Gaussian [52]. The IR intensities are relatively straightforward—they are related to the square of the dipole moment change with respect to Q, the relevant normal coordinate [53–56]; however, the Raman activities reported in the Gaussian output are not directly related to the observed differential Raman cross-sections $\partial\sigma_j/\partial\Omega$, i.e. the observed signal intensities. As reported in the Gaussian suite of programmes [52] the Raman activity for the jth normal mode S_j is given by Eq. (4) [57]. The activity contains the square of the derivative terms for the mean (isotropic) polarisability for mode j (a'^2_p) and the anisotropy (γ'^2_j) [58]. This parameter may be related to the observed Raman intensity in terms of the differential scattering cross-section as given in Eq. (5) [56] assuming that all appropriate experimental biases have been accounted for.

$$S = 45a'^2_j + 7\gamma'^2_j \tag{4}$$

$$\frac{\partial\sigma_j}{\partial\Omega} = \left(\frac{2^4\pi^4}{45}\right)\left(\frac{(\nu_0-\nu_j)^4}{1-\exp\left[\frac{-hc\nu_j}{kT}\right]}\right)\left(\frac{h}{8\pi^2 c\nu_j}\right)S_j \tag{5}$$

The first factor on the right-hand side of Eq. (5) contains constants, the second includes consideration of the fact that scattering is related to the fourth power of frequency with ν_0 being the laser frequency and ν_j the frequency of the jth mode and the population of the $\nu = 0$ state for the jth mode being accounted for in the denominator. The term $(h/8\pi^2 c\nu_j)S_j$ flows from the evaluation of the matrix elements for the first derivative of the Taylor expansion in polarisability.

The effect of this is that the Raman activity for higher frequency modes may be quite large but their scattering cross-section will be low—this is particularly true if FT-Raman measurements are made. This can be readily understood if we consider two Raman transitions a and b at 1000 and 3000 cm^{-1}, respectively; each with the same Raman activity. Application of Eq. (5) shows that if an FT-Raman experiment is conducted—in which $\nu_0 = 9398.5\,cm^{-1}$, corresponding to 1064 nm, then the observed relative scattering intensity has $(\partial\sigma_a/\partial\Omega) = 8.98 \times (\partial\sigma_b/\partial\Omega)$; that is, the lower frequency has almost an order of magnitude greater scattering intensity. In such cases it becomes very important to correctly evaluate the scattering intensities rather than simply use the Raman activities (Fig. 7).

In some cases the poor correlation between the observed and calculated Raman spectra can be informative as to the electronic nature of the compound of interest. For example, in a study of large dipole molecules, which have non-linear optical properties, McGoverin et al. [59] initially modelled these systems *in vacuo*—the results of the simulated spectra did not match the observed data in any satisfactory fashion; evidence for a lack of integrity of the calculated electronic structure. The poor correlation was manifested in two ways: firstly the frequencies calculated were at odds with the observed experimental data and secondly the intensities were also poorly correlated—notably the experimental Raman band at 1153 cm^{-1} was very weak in the simulated spectrum (see Fig. 7). A number of possible reasons for this discrepancy were investigated—these included the possible rotational conformers of the molecule and the introduction of a solvent field to better simulate the experiment (which was conducted in DMSO solution). Using a self-consistent reaction field method; the integral equation formalism polarisable continuum model, in which the solvent is considered as a continuum of a determined dielectric constant and the solute is within a cavity of the solvent and is modelled as a series of interlocked spheres [60,61], a much closer level of correlation was observed—importantly the strongest experimental Raman band at 1153 cm^{-1} was predicted at 1157 cm^{-1} with strong intensity. An analysis of the bond lengths in the structure showed that the com-

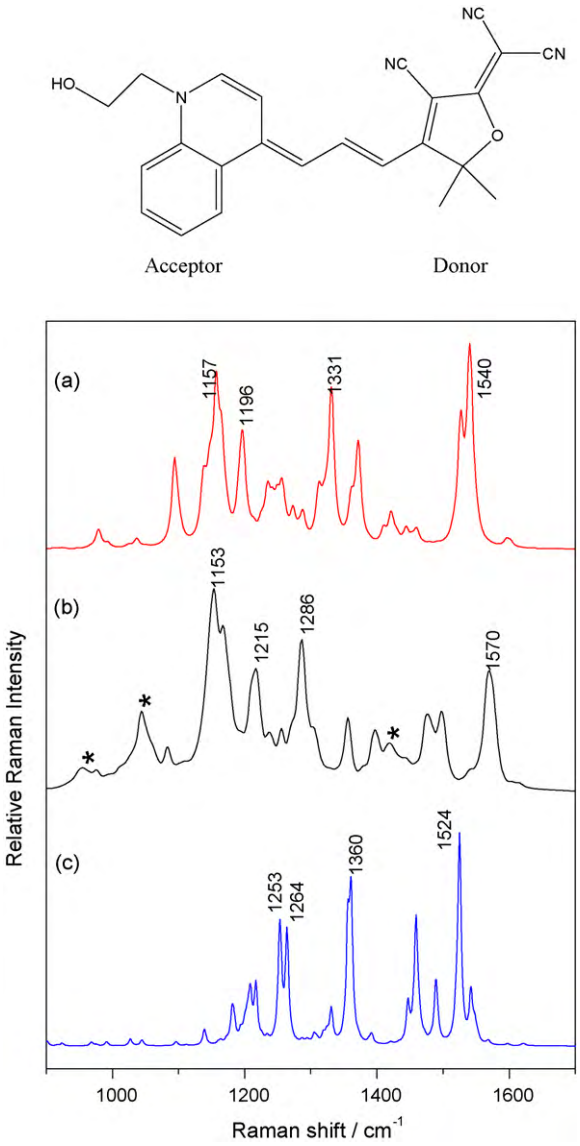

Fig. 7. Correlation of calculated with experimental parameters with and without consideration of solvent effects for the donor–π–acceptor compound depicted. (a) The calculated Raman spectrum in a DMSO solvent field. (b) The experimental FT-Raman spectrum carried out in DMSO. (c) The calculated Raman spectrum *in vacuo*.

pound was zwitterionic in nature rather than neutral—furthermore the hyperpolarisability (β) a key parameter in non-linear optical behaviour was much more accurately predicted in the calculation that had a better spectral correlation (the solvent field calculation) with β(experiment) = 440×10^{-30} esu, β(*in vacuo* calculation) = 19×10^{-30} esu and β(solvent field) = 445×10^{-30} esu.

4. Resonance Raman excitation profiles and bond length changes

In the study of metal polypyridyl complexes, resonance Raman spectroscopy has been used in a number of ways. At its simplest the technique has been applied to assist in the assignment of electronic transitions through a qualitative examination of the nature of the enhanced bands [62–65]. One of the early examples of using resonance Raman spectroscopy to analyse electronic transitions is a study of tris(α-diimine)iron(II) complexes including $[Fe(bpy)_3]^{2+}$ and $[Fe(phen)_3]^{2+}$ (phen = 1,10-phenanthroline; for ligands see Fig. 8) [66]. These studies demonstrated that the electronic spectra of these complexes in the visible region show

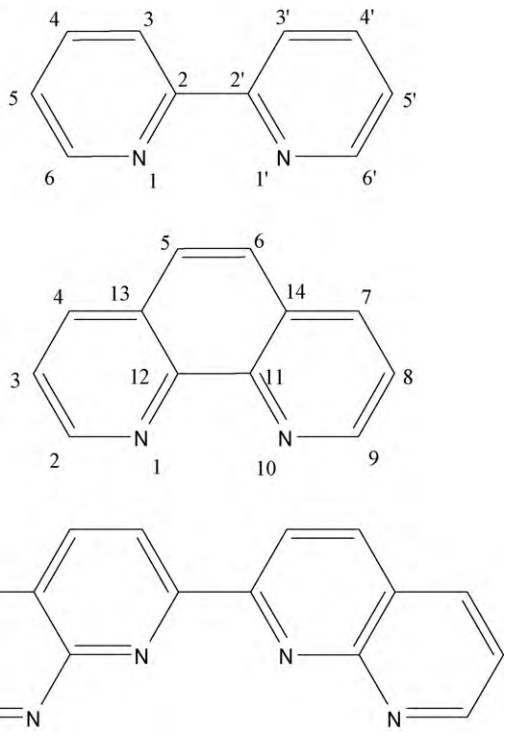

Fig. 8. 2,2-Bipyridine (top), 1,10-phenanthroline (middle) and 2,2′-bi-1,8-naphthyridine (bottom).

a single MLCT transition with a vibronic sideband. In a study of $[Ru(bpy)_2(L)]^{2+}$, where L = 2,2′-bi-1,8-naphthyridine and substituted ligands, the resonance Raman spectra showed enhancement of bpy modes with blue excitation, which disappeared as red excitation wavelengths were used—whereupon the observed spectra were dominated by 2,2′-bi-1,8-naphthyridine modes [67]. This was consistent with the presence of two MLCT transitions terminating on each of the ligands. Such studies are of value for assignment of transitions but they do not inform on the structural distortions associated with the respective transitions. This is possible but is not straightforward; in the next sections the methods for determining structure from resonance Raman data are illustrated with selected examples. In these we show how it is possible using a more quantitative analysis of the resonance Raman spectra to extract more insightful parameters, such as the dimensionless displacement (Δ) from the ground to resonant excited state.

4.1. Evaluation of structural distortion using the sum-over-states method

The work of Clark et al. demonstrated how effective resonance Raman excitation profiles could be in providing data on the structural distortions between the ground and the resonant electronic excited state. An excellent example of this is the use of resonance Raman excitation profiles to determine the geometry displacements in MnO_4^- [68]. Using Eq. (2) and considering A-term scattering the intensity of the resonance Raman transitions is simply the sum of Franck-Condon overlap factors. This is particularly well-suited to the examination of MnO_4^- because the resonance Raman spectrum is dominated by a single mode several overtones can be seen—thus the summation V is over about 7 vibrational levels and includes terms such as $\langle 1|V\rangle\langle V|0\rangle$, $\langle 2|V\rangle\langle V|0\rangle$ and the like. These can be computed following the work of Manneback [69] and

Nicholls [70]—for example:

$$\langle 0|0\rangle = e^{-\Delta^2/2}\left(\frac{\sqrt{\tilde{\nu}^e\tilde{\nu}^g}}{\tilde{\nu}^e+\tilde{\nu}^g}\right) \quad (6)$$

where Δ is the dimensionless shift parameter (Fig. 1) and $\tilde{\nu}^g$ and $\tilde{\nu}^e$ are the energies in wavenumbers of the mode of interest, for the ground- and excited-state surfaces, respectively.

Furthermore the displacement could be related to bond length changes by:

$$\Delta = \left(\frac{4\pi^2 c}{h}\right)^{1/2}\delta\mu^{1/2}\left(\frac{\tilde{\nu}_1^e\tilde{\nu}_1^g}{\tilde{\nu}_1^e+\tilde{\nu}_1^g}\right)^{1/2} \quad (7)$$

in which μ is the reduced mass of the vibrational mode (amu) and δ the displacement (pm).

An advantage of this is that overlap factors may be calculated, and from these data the resonance Raman excitation profiles may be modelled and compared to those observed. By looking at a system like MnO_4^- a strong series of overtone progressions can be observed in the resonance Raman spectra and these can be fitted by consideration of Franck-Condon overlap factors and estimates of δ and Γ (the dephasing term in Eq. (2)). In this case δ of approximately 10 pm provided a good fit to the data. A comprehensive review of the use of the sum-over-states approach is given in a review article by Clark and Dines [22].

4.2. Evaluation of Δ using the resonance excitation profiles and the time-dependent approach

Myers et al. [32] were the first to employ the time-dependent approach to calculate mode displacement in isoprene and hexatriene from pre-resonance spectra; later the application of wavepacket theory to coordination compounds was pioneered by Zink [68,71,72]. Due to the reasonable complexities of the examined molecules the short time dynamic limit (see Section 2) is appropriate to establish the Δ values for compounds with MLCT transitions [73,74].

A rather nice study using wavepacket theory was conducted by Doorn and Hupp [75] in which the intervalence charge-transfer (IVCT) dynamics of $[(CN)_5Ru\text{-}CN\text{-}Ru(NH_3)_5]^-$ was investigated using resonance Raman spectra. The electronic transition in this system is not MLCT but involves excitation from one metal centre to the adjacent centre.

$$\left[(CN)_5Ru^{II}(CN)Ru^{III}(NH_3)_5\right]^- \xrightarrow{h\nu} \left[(CN)_5Ru^{III}(CN)Ru^{II}(NH_3)_5\right]^-$$

By tuning the laser excitation into a post-resonance condition—that is using 514.5 nm excitation to probe an electronic transition at 647 nm, the short time dynamic approximation may be considered valid. This greatly simplifies the analysis of the data because the relative intensities (I) of the bands, a and b, may be related to their respective frequencies ($\omega = 2\pi\nu$ where ν is the frequency of the transition) and Δ values [28]. Thus:

$$\frac{I_a}{I_b} = \frac{\omega_a^2\Delta_a^2}{\omega_b^2\Delta_b^2} \quad (8)$$

Therefore by analysing the band intensities a series of relative Δ^2 values may be determined—this is useful, as by consideration of the electronic absorption bandwidth at $1/e$ the height of the band (W), the sum of Δ^2 may be determined [23,28,30,76] using [77]:

$$W = 2\left[\sum_j \Delta_j^2\left(\frac{\omega_j}{2\pi}\right)^2\right]^{1/2} \quad (9)$$

and then finally the Δ^2 may be converted to bond length changes *assuming* a local mode model—that is, by assigning each band to a specific set of bonds one can relate Δ^2 to bond length changes ($|\Delta a|$). Hence the change in bond length associated with mode j is given by [78]:

$$|\Delta a| = \sqrt{\frac{g_j\hbar}{\mu\omega_j}} \times |\Delta_j| \quad (10)$$

where g_j is the effective bond degeneracy for mode j and μ is the reduced mass. From this analysis, bond length changes could be determined for some of the bonds; for example the CN bridge was determined to distort by 0.046 Å. The greatest distortions were observed in the $M\text{–}C_{bridge}$ and $M\text{–}N_{bridge}$ linkages (>0.06 Å). As noted earlier, because it is the square of Δ that is being measured, the sign is undetermined—i.e. whether bonds are compressing or elongating is unknown from this type of analysis.

Pre-resonance Raman studies have been applied to the MLCT transitions in a number of instances. In a study of $[(NH_3)_4Ru(2,2'\text{-bpy})]^{2+}$ [79], which has an MLCT transition at 570 nm in hexamethylphosphoramide, measurements were made using excitation wavelengths 514.5, 647.1 and 676.4 nm (the second two wavelengths being pre-resonance conditions). Using the methodology outlined above for the $[(CN)_5Ru\text{-}CN\text{-}Ru(NH_3)_5]^-$ system the $|\Delta|$ values could be determined for the MLCT transition of $[(NH_3)_4Ru(2,2'\text{-bpy})]^{2+}$; on the basis of this method these distortions ($|\Delta|$) ranged from 0.1 to 1.4 which corresponds to bond length changes, $|\Delta a|$, of 0.002–0.08 Å. The authors note that in constructing $|\Delta a|$ they invoked a local mode approximation and this has some limitations with respect to a system in which delocalised normal modes would be more common than localised vibrations.

The forgoing examples used the short time dynamic approximation to relatively easily obtain values for the distortion of the excited state with respect to ground state. But these methods rely on being in pre- or post-resonance to provide accurate results and this method is not easily generally applied to many metal polypyridyl complexes. In a latter investigation on the $[(NH_3)_4Ru(2,2'\text{-bpy})]^{2+}$ Streiff and McHale [80] measured the resonance excitation profile of the complex in a series of solvents. By examining the resonance excitation profile it was possible to show that the complex revealed two overlapping transitions. This reveals one of the potential weaknesses in using the bandwidth of the electronic transition to set a bound value on the $\sum_j \Delta_j^2$ as shown in Eq. (9) [79], as implicit in this is the presence of only a single transition and that solvent effects are modest. Streiff and McHale [80] were able to fit the excitation profiles, absorption spectra and depolarisation ratios of the Raman transitions and demonstrate the presence of two overlapping transitions and the role of solvent in the observed spectra. The upshot of this was that the calculated $|\Delta|$ values required adjustment with the maximum displacement being 0.2 rather than 1.4 as previously reported [79].

Another interesting application of this is the study of mixed-valence excited-state (MVES) compounds, which are characterised by having two or more interchangeable excited-state configurations with different oxidation states. Several examples have been investigated by Zink, Nelsen and co-workers [81,82], including a transition-metal compound [83]. $[Ru(acp)_2(NH_3)_4]^{2+}$ (acp = 4-acetylpyridine) has two equivalent ligands available for MLCT excitation and thus two isoenergetic excited-state configurations with opposing Δ (see Fig. 9) may be formed. Due to coupling, these collapse into two adiabatic states of differing energy with the same equilibrium geometry. This is manifest in electronic absorption spectroscopy by splitting of a single band in the mono-acp compound into two bands in the bis-acp compound, separated by twice the coupling energy [82]. Although both *cis*- and *trans*-complexes exhibit coupling, the latter does not appear to show any splitting due to the dipole-forbidden nature of the higher-energy transition.

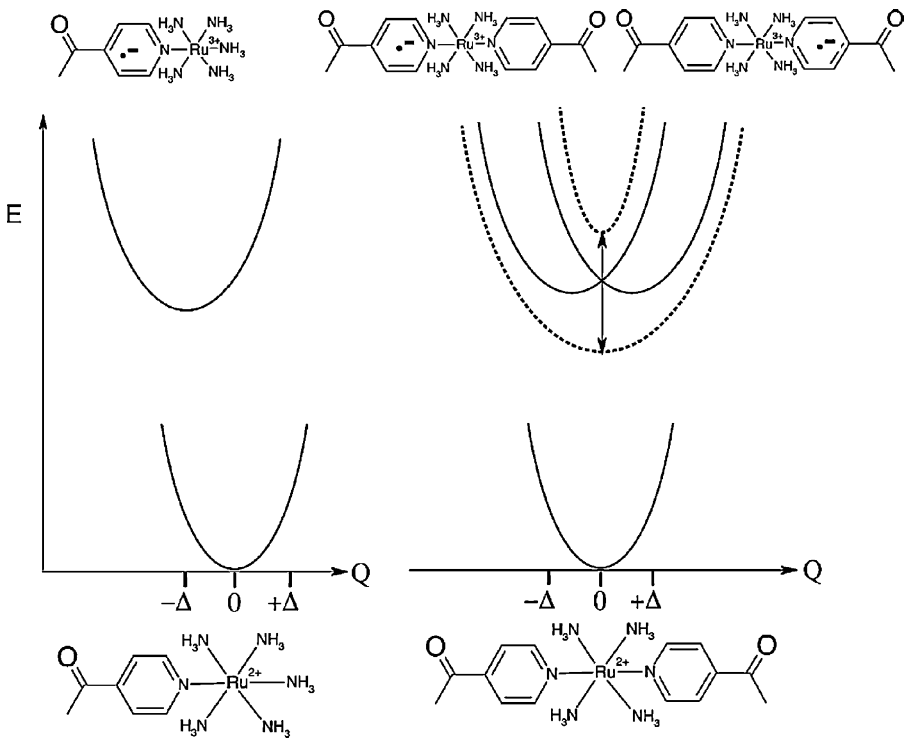

Fig. 9. The ground- and excited-state energy surfaces of $[Ru(acp)(NH_3)_5]^{2+}$ and *trans*-$[Ru(acp)_2(NH_3)_4]^{2+}$. In the latter, coupling of the excited-state configurations causes splitting in energy, which leads to two adiabatic potential surfaces.

Each of these states has been probed by resonance Raman spectroscopy and the peaks assigned using DFT calculations. Using Eq. (8) the dimensionless distortions were found to be greatest for the mode involving the metal–N (NH_3) bond, which is expected from earlier assignments in the literature [84] and akin to using reporter-ligands for the metal in IR spectroscopy (see Section 5). Other modes showing significant distortions occur at 1604 and 1210 cm^{-1}, which involve distortions of the C=C and C=N bonds.

One of the difficulties with these studies was that $|\Delta|$ could be evaluated but only rarely, for example in the case were modes are relatively simple in nature, could these be related to actual bond length changes. This is not to say that the determinations of $|\Delta|$ were not valuable, as they provided direct experimental parameters for reorganisation energies on going from ground to the resonant excited state—however in terms of structural changes they are often mute. However by combining DFT calculations and these data one can start to provide a picture of the excited-state distortions in terms of bond lengths for much more general systems, as has been successfully accomplished in organic systems [85].

4.3. Linking experimentally determined distortions with DFT

It is possible to establish the distortion of the resonant excited state from the ground state by analysis of the resonance Raman excitation profiles or by careful use of pre-resonance Raman intensities. Density functional theory may be used to establish the nature of the normal coordinates and indeed may be tested using normal Raman spectra; these two approaches may be brought together to permit the estimation of structure changes using a combination of experimental (Δ^2) and calculated (normal coordinate) parameters. In addition to attempting to relate the Δ^2 values to bond length changes it is possible to obtain the reorganisation energies for each mode through application of Eq. (11) [77] which relates the mode specific reorganisation energy (λ_j) to the frequency (ν_j) and displacement (Δ_j).

$$\lambda_j = \frac{\nu_j \Delta_j^2}{2} \tag{11}$$

This is useful because the electron-transfer properties of a charge-transfer excitation comprise a total reorganisation energy which is the sum of the inner sphere reorganisation $\left(\lambda_i = \sum_j \lambda_j\right)$ and the outer sphere reorganisation (λ_o, related to the inhomogeneous broadening).

The structural changes attendant upon MLCT excitation were investigated by Waterland et al. in a study of $[Cu(pqx)(PPh_3)_2]^+$ (pqx is 2-(2′-pyridyl)quinoxaline) [86]. The compound was modelled using DFT. The correlation between experimental and calculated Raman data had a mean absolute deviation of 7 cm^{-1} and the ligand structure bonds were calculated to within 0.03 Å of the crystal structure. The electronic absorption spectrum was modelled with TD-DFT revealing a MLCT transition of appreciable intensity in the visible region at 419 nm—the observed band in CH_2Cl_2 occurs at 430 nm. Importantly only one MLCT transition was calculated in the visible region—hence the interference effects prevalent in studies of $[(NH_3)_4Ru(2,2'\text{-bpy})]^{2+}$ discussed in Section 4.2 are not likely to be observed in this system. The resonance Raman spectra were satisfactorily fitted using wavepacket modelling which provided a number of interesting insights: (1) the overall reorganisation energy for the MLCT excitation was roughly equal between inner sphere (solute bonding) and outer sphere (solvent) and was approximately 3500 cm^{-1} in each case. This value is not unexpected as the MLCT transition formally oxidises the metal from copper(I) to copper(II) which leads to a significant alteration in bond order around the metal but also a reorganisation of the solvent shell as the metal expands to five-coordinate geometry with oxidation [87–89]; (2) the mode specific reorganisation energies are found in two modes that have bands at 529 and

1475 cm^{-1}; these correspond to bond displacements of 0.15 and 0.1 Å, respectively. These are consistent with the calculated structural changes that occur in the triplet state of $[Cu(pqx)(PPh_3)_2]^+$ and the reduced species $[Cu(pqx)(PPh_3)_2]^0$, in which the reducing electron occupies a ligand-based MO as occurs in the ^{3}MLCT excited state.

In a related study $Re(pqx)(CO)_3Cl$ was examined [90]. In this case dimensionless displacements along bond lengths are reported based on transforming the dimensionless Δ values. This is a very difficult process as for N resonance Raman bands used there are 2^N possible combinations of displacements consistent with the observed intensities. This was handled by calculating the triplet structure for $Re(pqx)(CO)_3Cl$, assuming that structure at least distorted in a similar direction to the resonant ^{1}MLCT state and used the observed bond length changes to derive plausible or at least consistent bond length distortions. This analysis is consistent with other experiments that have attempted to determine bond length changes, notably the work of Morrsion et al. [91,92] in which the bond lengths for the CO ligands in metal carbonyls such as $Re(CO)_3(bpy)Cl$ were estimated using an empirical relationship of the form $r_{CO} = 1.6916–0.1736\ln(k_{CO})$ (r/Å, k/mdyn Å^{-1}) akin to Badger's rule [93,94], and the shifts in the carbonyl vibration were found on going from the ground to ^{3}MLCT excited state. The study of $Re(pqx)(CO)_3Cl$ [90] demonstrates rather well the limitations of resonance Raman excitation profile studies in metal polypyridyl systems—although Δ^2 may be established with reasonable confidence the ability to go beyond that and determine bond length and angle changes is somewhat limited and probably not generally applicable using transformation methods as outlined in this study. The potential to obtain structural information about the resonant excited state is realisable through application of density functional theory as outlined in Section 4.4. Furthermore the use of Δ^2 values, determined experimentally to obtain reorganisation energies for photoexcitation, is an important area.

An example of how Δ^2 and the reorganisation energies they relate to are useful in understanding dynamics is given in a study of the short time behaviour of a series of $Cu^I(L)_2^+$ complexes, in which L = 2,2′-bipyridine (bpy), 1,10-phenanthroline (phen) and 2,9-dimethyl-1,10-phenanthroline (dmp) (ligands in Fig. 8) [95]. Copper(I) polypyridyl complexes are somewhat atypical in that in their MLCT excited states the coordination number of the copper increases, as it is formally oxidised from +1 to +2; this coordination sphere expansion causes the MLCT excited-state lifetime to be extremely sensitive to solvent. This model was termed the exciplex-model in which the five-coordinate solvent adduct species lowers the energy of the excited state such that the non-radiative decay rate is greatly increased [89]. For example in non-coordinating solvents, such as CH_2Cl_2, $[Cu(dmp)_2]^+$ has an emissive state with a lifetime of about 90 ns, but in MeCN the emission is quenched [96]. Compelling evidence exists for this model through the direct observation of an expanded coordination sphere [97,98] and the fact that excited-state lifetimes may be tuned with judicious use of substituents about the metal centre [87,88]. Although the existence of the exciplex is well established, the dynamics of its formation are less well understood. A series of theoretical studies predict a blue-shift in transient absorption spectra as a consequence of an increase in the HOMO-LUMO gap through the flattening from tetrahedral geometry (Fig. 10) [99,100]. In a study of the ultrafast transient absorption spectra of $[Cu(dmp)_2]^+$ such a blue-shift was indeed observed upon photoexcitation, with 10–20 ps duration [97]; this was reasoned to be due to the prompt flattening of the structure, presumably from the initially populated surface—thus the FC state contained a distortion along a flattening coordinate. However a subsequent study by Shaw et al. [101] observed the 10–20 ps transient for both $[Cu(dmp)_2]^+$ and the more sterically hindered $[Cu(dpp)_2]^+$ (where dpp = 2,9-diphenyl-1,10-phenanthroline)—the

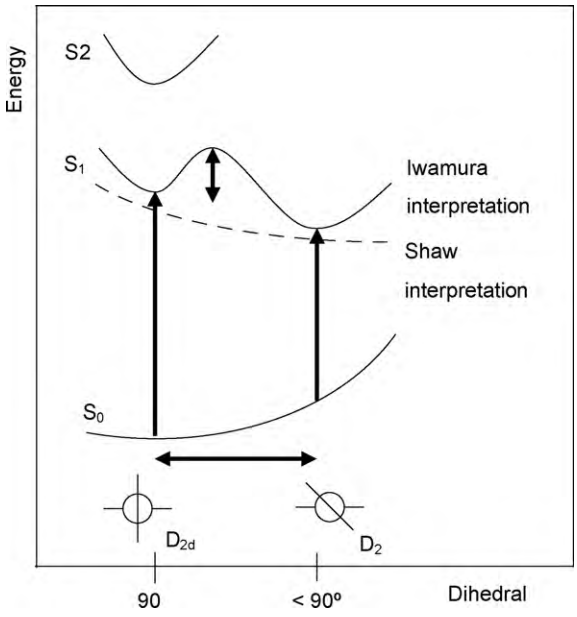

Fig. 10. Energy changes in the excited state of $[Cu(dmp)_2]^+$ as a function of interligand dihedral angle.

invariance of this transient feature suggested that it was not related to flattening dynamics but was the intersystem crossing process from ^{1}MLCT to ^{3}MLCT states. Nonetheless Shaw also observed an 80 fs transient that was attributed to the flattening distortion—this again suggests that the FC state contains a flattening coordinate. In a detailed study by Iwamura et al. [102] three distinct spectral features were identified in the relaxation of $[Cu(dmp)_2]^+$. The optical spectrum of $[Cu(dmp)_2]^+$ contains two MLCT transitions termed S_1 and S_2 (Fig. 10). The dynamics showed that for population of the S_2 state a 45 fs transient was observed that was structurally very similar to the ground state, in which the ligands remained perpendicular (no flattening was observed); for population of the S_1 state the initial excited state was structurally undistorted—distortion to a flattened structure occurred over 660 fs. A key finding of this work was that the initially formed S_1 state, termed S_1(perpendicular), is a weakly bound state, having a barrier to formation of the flattened structure, the S_1(flattened) state. The resonance Raman excitation profiles offer an excellent way to test such conflicting results; if the S_1 state contains a flattening coordinate in the FC region then associated enhancement of modes will be observed; if it does not then no torsion modes will be enhanced. In the study of the resonance Raman excitation profiles three complexes were measured; these complexes were different in terms of their flexibility and capability to form the five-coordinate species with $[Cu(bpy)_2]^+$ being the most flexible and $[Cu(dmp)_2]^+$ the least. Taking into account the potential pitfalls of having two interfering transitions [80], the data may be fitted and reveal the mode specific reorganisation energies for the three compounds. The results show that the enhancements are predominantly delocalised ligand modes and no substantive evidence for ligand torsional modes are obtained—on this basis it would seem that the resonance Raman excitation profiles are supportive of the model proposed by Iwamura et al. [102]. Furthermore it was found that the overall vibrational reorganisation energies were approximately 1000 cm^{-1} for $[Cu(dmp)_2]^+$ and $[Cu(phen)_2]^+$, but 2000 cm^{-1} for $[Cu(bpy)_2]^+$; which is consistent with the fact that the reduction of the ligand upon photoexcitation has a greater effect on the structure of bpy than either phen or dmp [95].

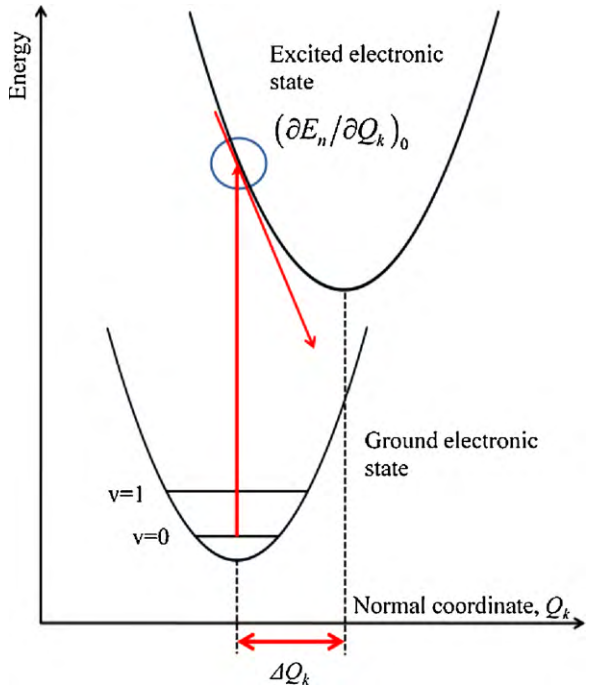

Fig. 11. Relation of ΔQ_k to the excited-state gradient along a dimensional normal coordinate.

4.4. Direct calculation of dimensionless displacements

In the forgoing, experimental data have been used to fit various parameters concerned with electronic transitions; these include, homogeneous and inhomogeneous bandwidths, the transition energies and the dimensionless displacements along normal coordinates associated with the electronic excitation. The ability to calculate the vibrational spectra with some accuracy has meant that it is possible to extract structural information, as the displacements along normal coordinates may be converted to displacements along bond lengths and angles [90]. However it should be possible to calculate the resonance Raman intensities if there is sufficient knowledge of the electronic transition and the normal modes. This idea was discussed by Hudson et al. [31] in which the resonance Raman spectra of a number of imidazole and its protonated and deuterated analogues were examined. At the heart of this method is the recognition that in wavepacket theory as expounded by Heller [28], in the short time dynamic limit, the intensity of a Raman band (i) related to the gradient of the potential energy surface (given as $(\partial E/\partial Q_k)_0$; see Fig. 11). Despite the successful application of this strategy to the resonance Raman spectra of imidazole the authors recognize some caveats in this approach: (1) the presence of a number of close-lying resonant states makes the calculation more difficult, as it will be unclear which state is contributing to the resonant transition; (2) it is assumed that the short time dynamic limit holds–this is a very reasonable approximation for large molecules and is widely observed.

This original concept has been developed by Neese [103] and implemented in the ORCA suite of programs [104]. The key to its success is the calculation of the resonant excited-state geometry relative to the ground state.

This is made much more reliable than the initial Hudson studies because the ORCA suite of programmes are extremely effective at determining the excited-state energy gradients at the ground-state geometry. The displacements are then given by (Fig. 11) [105,106]:

$$\Delta_{Q,k}(n) = -\omega_k^{-2}(n)\left(\frac{\partial E_n}{\partial Q_k}\right)_0 \quad (12)$$

where $\Delta_{Q,k}(n)$ is the displacement (Δ) along the kth normal mode for the nth excited state, $\omega_k(n)$ is the vibrational frequency of the kth mode in the nth excited state (normally taken to be equivalent to the ground-state vibrational energy) and $(\partial E_n/\partial Q_k)_0$ is the gradient of the nth excited state at the ground-state geometry. This method has been successfully applied to the study of the resonance Raman spectra of transition-metal bis-dithiolenes [107].

These methods represent a hybrid in which computational chemistry is used to derive the displacements and then wavepacket theory is applied with varying degrees of rigour to extract the resonance Raman intensities. An alternate method is to directly calculate the polarisabilities for on resonance conditions—this is possible using response functions [108] but is at a rather early stage of development. However, it is likely that these methods will become more common as the implementation improves. At present calculations have focused on relatively simple systems, such as pyridine [109], uracil and pyrene [110].

5. Time-resolved methods—direct observation of the excited state

Rather than the indirect analysis of the excited state described in Sections 2–4, one can perform a direct analysis of transient-species by using time-resolved or transient resonance Raman (TR^3 and TR^2, respectively) spectroscopy. Both techniques involve the use of a laser pulse to pump the sample in order to photogenerate excited-state molecules, followed by Raman scattering from this and subsequently evolving states. Here we will refer to the thermally equilibrated excited (THEXI) state, which is probed in a majority of TR^2 and TR^3 experiments. This state is usually formed from the initial ^{1}MLCT state, after vibrational relaxation and intersystem crossing to a triplet system, generally on a femto or picosecond timescale (*vide infra*). TR^3 lends itself to the elucidation of excited-state structure rather well compared to techniques such as transient absorption and emission, as changes in electronic structure have a profound effect on the vibrational modes observed. The THEXI state is particularly interesting from a photochemistry point of view since it represents a high-energy isomer of the parent species, a fact that is potentially useful in applications such as photosensitisers in the photocatalytic reduction of CO_2 or in water-splitting devices [111,112]. Furthermore, it can play a part in the electron-transfer reactions between a dye molecule and TiO_2 nanoparticle in dye-sensitised solar cells (DSSCs). While charge-injection into the valence-band (VB) of TiO_2 occurs from the ^{1}MLCT state on a femtosecond-timescale [113,114], if intersystem crossing is fast enough, population of the ^{3}MLCT state can take place preferentially [115]. In that case charge-injection can occur on a much longer timescale and the structure, energetics and lifetime of the THEXI state become very important in understanding the functioning (or lack thereof) of a device.

In TR^3, pumping and probing of the sample is carried out by separate lasers, which are synchronised with a gated camera to observe Raman emission only during the "probe" window. The advantages of TR^3 are threefold: (1) using appropriate laser-pulse durations and timings, a variety of timescales can in theory be probed. This enables the study of the THEXI state or pre-THEXI processes [116]. (2) The pump and probe wavelengths can be adjusted independently from each other. This is important as photoexcitation often leads to different absorption properties and thus resonance-enhancement of Raman scattering in the ground state does not guarantee the same in the excited state at the same exci-

tation wavelength. Changing the probe wavelength can therefore help elucidate excited-state dynamics [12]. (3) Emission before and after the event of interest is rejected, potentially increasing the signal to noise ratio and decreasing spectral contributions from the ground state. In contrast, TR^2 spectroscopy uses a single laser pulse to pump and probe the sample and a standard (non-gated) detector. Such experiments are very effective for probing the THEXI-states of transition-metal compounds, provided the lifetime is comparable to or longer than the duration of the laser pulse and the photon flux of the pulse is sufficient to generate appreciable excited-state concentrations. The appeal of TR^2 experiments is the relatively straightforward setup compared to the time-resolved approach. Since a majority of TR^3 experiments are carried out on the THEXI state, TR^2 is a popular alternative for some systems.

In MLCT states the key species is M^+L^- in which the metal is formally oxidised and the ligand reduced, thus spectral features associated with the M^+ or L^- moieties are of interest. Generally TR^2 and TR^3 methods are informative about the L^- species (or more correctly $L^{\bullet -}$) as these species have electronic absorptions in the visible region and hence show resonance-enhancements in the excited state which is often overlapping with the ground-state MLCT transition. This makes such systems amenable to TR^2 studies. It is possible to probe the changes in the metal centre—that is the formation of the M^+ state, if appropriate reporter groups, such as CO or CN^-, are bound to the metal. However, in general these bands are not resonantly enhanced in the excited state and are comparatively weaker than the $L^{\bullet -}$ features [117]. Indeed the advent of time-resolved infrared methods [92,118,119] which directly probe CO or CN^- vibrations negates the use of excited-state resonance Raman studies to examine the M^+.

Arguably the most intensely studied compound using Raman spectroscopy is $[Ru(bpy)_3]^{2+}$, after it was found that its excited-state potential and relatively long-lived ^{3}MLCT state could be used to split water [120,121]. The excited state involves an electron-transfer from the metal to the ligand; however, the localisation of the excited electron in $[Ru(bpy)_3]^{2+}$ and related compounds has been the subject of extensive debate [11,116,122–124]. In a landmark paper, Dallinger and Woodruff [11] used TR^3 to show that photoexcitation can be viewed as the reaction $[Ru^{II}(bpy)_3]^{2+} \rightarrow [Ru^{III}(bpy)_2(bpy^{\bullet -})]^{2+}$, that is, oxidation of the metal and reduction of a single bipyridine ligand, at least on a timescale of nanoseconds and longer. Peaks due to the excited-state bipyridine radical anion were seen along with ground-state features, indicating that both species are present in the sample (i.e. a heteroleptic complex is formed). This would not be seen if the excited electron was delocalised across all three bipyridines. Similar characteristic peaks were found for bipyridine complexes of other metals [10,125]. A more recent experiment by Henry and co-workers [116] has examined the vibrational activity of $[Ru(bpy)_3]^{2+}$ just after photoexcitation with TR^3 spectroscopy. Using a 400 nm pump laser and a variety of probe lasers, a growth of excited-state features with a time-constant of *ca.* 10 ps is observed. This is invariant with the counter-anion or the solvent used, suggesting that solvent-reorganisation is not involved in the rate-limiting process. One of the solvents used is acetonitrile, with a solvent-reorganisation rate of *ca.* 200 fs, therefore the longer timescales observed are expected [126]. The ps evolution of THEXI features is supported by time-resolved emission studies as well as vibrational cooling on a 20 ps scale of $Re(bpy)(CO)_3Cl$ observed by Alsindi Wassim and co-workers [127]. However the data are at odds with a number of transient absorption [128], time-resolved femtosecond stimulated Raman [129] and broadband femtosecond fluorescence studies [130], which predict far more rapid vibrational relaxation times, albeit without agreement. In light of this the Henry study [116] interpreted the fast process as ISC, occurring in *ca.* 200 fs, and the slower process as vibrational relaxation of the ^{3}MLCT state to give the THEXI state, occurring in *ca.* 10 ps. This conclusion has implications on the charge-injection dynamics in DSSCs. While the debate on pre-THEXI processes of $[Ru(bpy)_3]^{2+}$ and related complexes is an ongoing one, these efforts are useful in demonstrating the time-resolution capabilities of TR^3 while maintaining the ability to gain structural insight through molecular vibrations.

In addition to the exciplex-model discussed above (Section 4.3) the THEXI-states of complexes based on $[Cu(dmp)_2]^+$ have also been examined, using transient and time-resolved resonance Raman techniques [12,131–133]. Like $[Ru(bpy)_3]^{2+}$ derivatives, synthesis of these compounds is reasonably straightforward and they exhibit interesting photophysical properties. The THEXI-lifetimes of $[Cu(phen)_2]^+$-based complexes in deaerated solutions of poor donor solvents (such as CH_2Cl_2) can approach 1 μs [48,134] making them well-suited to such analysis, and can be readily tuned by substituents. Gordon and McGarvey [12] used TR^2 spectroscopy to demonstrate that in the excited state of $[Cu(dmp)_2]^+$ the photoelectron is localised on one of the dmp-ligands, analogous to the case of $[Ru(bpy)_3]^{2+}$ shown above. For $[Cu(dmp)_2]^+$ in CH_2Cl_2 using pulsed excitation at 447.2 nm, features are observed that are reminiscent of the excited-state spectrum of $[Cu(dmp)(PPh_3)_2]^+$, while ground-state features diminish in intensity. In MeOH all features observed are of the ground state, as the lifetime of the complex in this solvent is shorter than the laser-pulse duration (see above). No excited-state features were observed at 503 or 532 nm [135] excitation in either solvent, although the ground-state features diminished somewhat. Such bleaching behaviour can be observed when the excited-state species, in this case the radical anion of dmp, has a low absorption coefficient at the probe wavelength used, and thus shows little resonance-enhancement. In a study [131] on $[Cu(L)_2]^+$ and $[Cu(L)(PPh_3)_2]^+$, where L = 2,2′-biquinoline (biq) or 6,7-dihydro-5,8-dimethyldibenzo[b,j][1,10]-phenanthroline (DMCH),

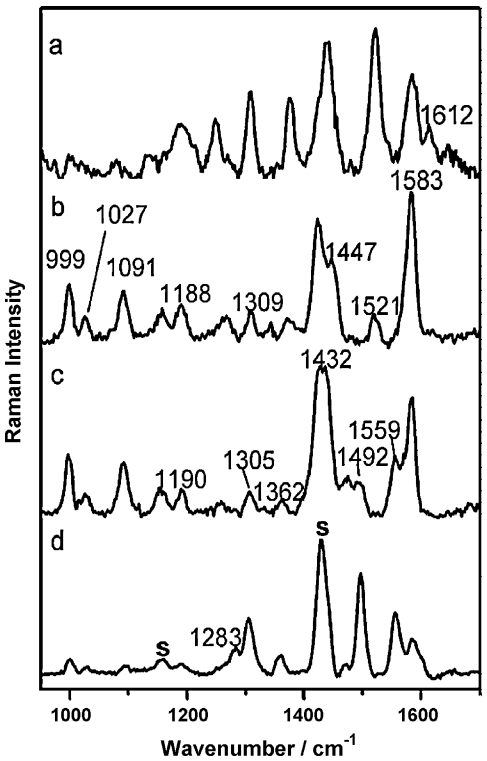

Fig. 12. Resonance Raman spectra of $[Cu(tem)(PPh_3)_2]^+$ (traces a and b) and its perdeuterated analogue (traces c and d). Traces a and d show resonance Raman spectra acquired at 356.4 nm while transient resonance Raman spectra acquired at 354.7 nm are shown in the middle.

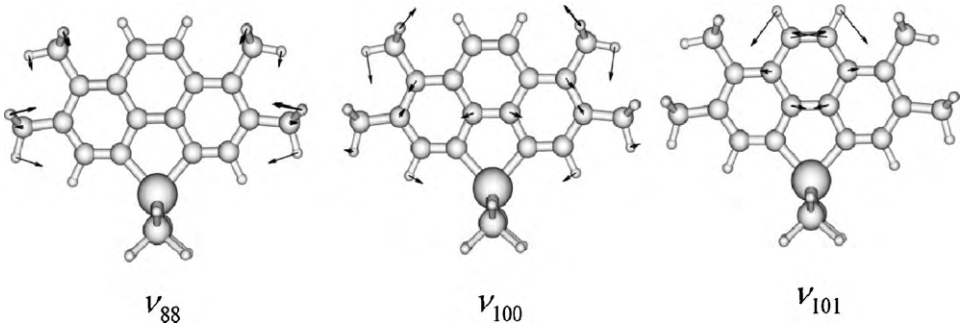

Fig. 13. Calculated normal modes for peaks in the spectrum of $[Cu(tem)(PPh_3)_2]^+$. ν_{expt}/ν_{calc} for ν_{88}, ν_{100} and ν_{101} are 1447/1454, 1521/1541 and 1583/1572, respectively.

observation of the resonance Raman signals of the radical anion, $L^{\bullet-}$, was attempted in two ways: (1) using transient resonance Raman the species are optically generated via an MLCT transition and probed and (2) using an optically transparent thin-layer electrode (OTTLE) cell the species are electrochemically generated and probed using regular resonance Raman spectroscopy. It was found that for the homoleptic complexes the first electrochemical reduction occurs on the metal to give $[Cu(0)(L)_2]$, while the second reduction produces a radical anion species, as evidenced by UV–visible spectroscopy as well as colour changes. A rather unusual reduction sequence is evidenced by resonance Raman: the second reduction results in the formation of $[Cu(I)(L^{\bullet-})_2]^-$ as opposed to a heteroleptic Cu(0) species; that is, oxidation of the metal and reduction of each ligand. Furthermore, comparison of the TR^2 spectra of the mono-ligand with the corresponding mixed-ligand complexes reveals very similar excited-state features, which is evidence for localisation of the optical electron.

While the $L^{\bullet-}$ species generated through different processes are generally comparable in their resonance Raman spectra, a significant difference occurs for the band at *ca.* 1570 cm^{-1} in the TR^2, which is shifted to *ca.* 1585 cm^{-1} for the electrochemically reduced homoleptic complexes. A possible reason for this was suggested to be the differing oxidation states of the metals (Cu(I) for electrochemical compared to Cu(II) for MLCT) having differing effects on the ligands.

In more recent studies [46,48], DFT methods were employed to model the radical anions of similar complexes to compare to TR^2 spectra, with the aim of providing more detailed assignments of excited-state vibrational features. It was possible to correlate peaks in the excited-state spectra with specific molecular vibrations. Fig. 12 shows the ground- and excited-state spectra of $[Cu(tem)(PPh_3)_2]^+$ (tem = 3,4,7,8-tetramethyl-1,10-phenanthroline) and $[Cu(d_{16}\text{-tem})(PPh_3)_2]^+$. Comparing traces a and d it is obvious that deuteration has a marked effect on the spectra of the complexes. This is useful in distinguishing the PPh_3 ligand stretching modes, as they are not assumed to be influenced greatly by deuteration of the tem unit.

Comparing the ground- and excited-state spectra a and b, respectively, new peaks or increased intensities are seen (marked peaks), while the features such as the peak at 1612 cm^{-1} are bleached with respect to the solvent, evidence that a significant amount of excited state is formed. Using DFT calculations of the radical anions of the complexes, the vibrational normal modes of the excited-state compounds were found, for example the modes at 1447, 1521 and 1583 cm^{-1} of $[Cu(tem)(PPh_3)_2]^+$ shown in Fig. 13. Comparison of these with modes corresponding to equivalent bands in the spectrum of $[Cu(tem)(PPh_3)_2]^+$ provided evidence for the differing excited-state symmetries of b_1 and a_1 for the phen and tem compounds, respectively.

While the calculated and experimental excited-state spectra generally show reasonable agreement, the mean actual deviations are higher than for ground-state spectra.

A better approach, albeit a more computationally intensive one, is to calculate the triplet state of the complex. In a study on $[Re(NCS)(CO)_3(L)]$, where L = bpy or di-^{i}Pr-*N*,*N*-1,4-diazabutadiene (^{i}Pr-DAB), Vlcek and co-workers [13,17] compared time-resolved IR data to calculated triplet-state spectra and found good correlation between the two. Of course, using IR spectroscopy also has the advantage that, in a good calculation, calculated and measured intensity patterns are expected to be similar. The comparison of resonance Raman signals is more problematic.

6. Conclusions and future outlook

This is a brief overview of how resonance Raman techniques may be applied to transition-metal complexes. It is shown how resonance Raman, TR^2 and TR^3 can be used to elucidate the excited-state dynamics of some select examples; however applications are obviously more far-reaching. Several reviews [43,122,136,137] have been and are still being written on the topic; testament to the continuing proliferation and utility of these techniques. In terms of resonance Raman spectroscopy as a probe of the FC state of MLCT transitions it appears that the application of wavepacket analysis to resonance excitation profiles, in concert with DFT calculations, is a very useful way to establish reorganisation energies of the resonant excited state. By using "hybrid methods" such as TD-DFT, calculations on equilibrium and near-equilibrium structures DFT can provide qualitative agreement with the structural resonance Raman spectra and this allows for an evaluation of displacements for the resonant excited state. In the future it appears that direct calculation of the resonant Raman intensities is possible and will be implemented in the coming years. In terms of pulsed Raman methods, such as TR^2 and TR^3 these remain simple and useful experiments for the analysis of THEXI MLCT states; their utility in examining $L^{\bullet-}$ species make them complimentary to time-resolved infrared methods, which have developed very significantly in the last decade.

Acknowledgements

The support of the Foundation of Research Science and Technology, the Royal Society of New Zealand (Marsden Fund) and the MacDiarmid Institute for Advanced Materials and Nanotechnology is gratefully acknowledged. RH thanks the University of Otago for a postgraduate scholarship.

References

[1] M.K. Nazeeruddin, C. Klein, P. Liska, M. Graetzel, Coord. Chem. Rev. 249 (2005) 1460.
[2] A. Islam, H. Sugihara, H. Arakawa, J. Photochem. Photobiol. A 158 (2003) 131.
[3] T. Renouard, R.A. Fallahpour, M.K. Nazeeruddin, R. Humphry-Baker, S.I. Gorelsky, A.B.P. Lever, M. Graetzel, Inorg. Chem. 41 (2002) 367.
[4] K. Hara, H. Sugihara, Y. Tachibana, A. Islam, M. Yanagida, K. Sayama, H. Arakawa, G. Fujihashi, T. Horiguchi, T. Kinoshita, Langmuir 17 (2001) 5992.
[5] G. Sauve, M.E. Cass, G. Coia, S.J. Doig, I. Lauermann, K.E. Pomykal, N.S. Lewis, J. Phys. Chem. B 104 (2000) 6821.
[6] A. Islam, H. Sugihara, K. Hara, L. Pratap Singh, R. Katoh, M. Yanagida, Y. Takahashi, S. Murata, H. Arakawa, New J. Chem. 24 (2000) 343.
[7] U. Bach, D. Lupo, P. Comte, J.E. Moser, F. Weissortel, J. Salbeck, H. Spreitzer, M. Gratzel, Nature 395 (1998) 583.
[8] B. O'Regan, M. Graetzel, Nature 353 (1991) 737.
[9] A.W. Adamson (Ed.), J. Chem. 60 (1983) 797.
[10] P.G. Bradley, N. Kress, B.A. Hornberger, R.F. Dallinger, W.H. Woodruff, J. Am. Chem. Soc. 103 (1981) 7441.
[11] R.F. Dallinger, W.H. Woodruff, J. Am. Chem. Soc. 101 (1979) 4391.
[12] K.C. Gordon, J.J. McGarvey, Inorg. Chem. 30 (1991) 2986.
[13] A. Vlcek, S. Zalis, Coord. Chem. Rev. 251 (2007) 258.
[14] D.M. Dattelbaum, R.L. Martin, J.R. Schoonover, T.J. Meyer, J. Phys. Chem. A 108 (2004) 3518.
[15] D.M. Dattelbaum, K.M. Omberg, P.J. Hay, N.L. Gebhart, R.L. Martin, J.R. Schoonover, T.J. Meyer, J. Phys. Chem. A 108 (2004) 3527.
[16] D.G. Thompson, J.R. Schoonover, C.J. Timpson, T.J. Meyer, J. Phys. Chem. A 107 (2003) 10250.
[17] A.M.B. Rodriguez, A. Gabrielsson, M. Motevalli, P. Matousek, M. Towrie, J. Sebera, S. Zalis, A. Vlcek Jr., J. Phys. Chem. A 109 (2005) 5016.
[18] A.C. Albrecht, J. Chem. Phys. 34 (1961) 1476.
[19] A.Y. Hirakawa, M. Tsuboi, Science 188 (1975) 359.
[20] M.W. George, F.P.A. Johnson, J.R. Westwell, P.M. Hodges, J.J. Turner, J. Chem. Soc., Dalton Trans. (1972–1999) (1993) 2977.
[21] S.L. Howell, S.M. Scott, A.H. Flood, K.C. Gordon, J. Phys. Chem. A 109 (2005) 3745.
[22] R.J.H. Clark, T.J. Dines, Angew. Chem. Int. Ed. 98 (1986) 131.
[23] S.-Y. Lee, E.J. Heller, J. Chem. Phys. 71 (1979) 4777.
[24] E.J. Heller, R. Sundberg, D. Tannor, J. Phys. Chem. 86 (1982) 1822.
[25] A.B. Myers, R.M. Hochstrasser, J. Chem. Phys. 87 (1987) 2116.
[26] A.B. Myers, Acc. Chem. Res. 30 (1997) 519.
[27] A.B. Myers, R.A. Mathies, in: T.G. Spiro (Ed.), Raman Spectra and the Conformations of Biological Macromolecules, Wiley, New York, 1987, p. 1.
[28] E.J. Heller, Acc. Chem. Res. 14 (1981) 368.
[29] E.J. Heller, Faraday Discuss. Chem. Soc. (1983) 141.
[30] D.J. Tannor, E.J. Heller, J. Chem. Phys. 77 (1982) 202.
[31] B.S. Hudson, L.M. Markham, J. Raman Spectrosc. 29 (1998) 489.
[32] A.B. Myers, R.A. Mathies, D.J. Tannor, E.J. Heller, J. Chem. Phys. 77 (1982) 3857.
[33] S.J. Lind, T.J. Walsh, A.G. Blackman, M.I.J. Polson, G.I.S. Irwin, K.C. Gordon, J. Phys. Chem. A 113 (2009) 3566.
[34] A.M. Moran, C. Delbecque, A.M. Kelley, J. Phys. Chem. A 105 (2001) 10208.
[35] C.E. Foster, B.P. Barham, P.J. Reid, J. Chem. Phys. 114 (2001) 8492.
[36] D.S. Egolf, M.R. Waterland, A.M. Kelley, J. Phys. Chem. B 104 (2000) 10727.
[37] E. Shorr, A.M. Kelley, Phys. Chem. Chem. Phys. 9 (2007) 4785.
[38] S.L. Howell, K.C. Gordon, M.R. Waterland, K.H. Leung, D.L. Phillips, J. Phys. Chem. A 110 (2006) 11194.
[39] E.B. Wilson Jr., J.C. Decius, P.C. Cross, Molecular Vibrations, McGraw-Hill, New York, 1955.
[40] D.P. Strommen, P.K. Mallick, G.D. Danzer, R.S. Lumpkin, J.R. Kincaid, J. Phys. Chem. 94 (1990) 1357.
[41] B.J. Matthewson, A. Flood, M.I.J. Polson, C. Armstrong, D.L. Phillips, K.C. Gordon, Bull. Chem. Soc. Jpn. 75 (2002) 933.
[42] M.R. Waterland, K.C. Gordon, J. Raman Spectrosc. 31 (2000) 243.
[43] W.R. Browne, J.J. McGarvey, Coord. Chem. Rev. 250 (2006) 1696.
[44] Strictly speaking the correlation is made between the experimental wavenumbers and those calculated subsequent to empirical scaling.
[45] A.P. Scott, L. Radom, J. Phys. Chem. 100 (1996) 16502.
[46] S.L. Howell, K.C. Gordon, J. Phys. Chem. A 108 (2004) 2536.
[47] S.L. Howell, K.C. Gordon, J. Phys. Chem. A 110 (2006) 4880.
[48] S.L. Howell, K.C. Gordon, J. Raman Spectrosc. 39 (2008) 813.
[49] S.L. Howell, K.C. Gordon, J.J. McGarvey, J. Phys. Chem. A 109 (2005) 2948.
[50] P.J. Walsh, K.C. Gordon, N.J. Lundin, A.G. Blackman, J. Phys. Chem. A 109 (2005) 5933.
[51] S.L. Howell, B.J. Matthewson, M.I.J. Polson, A.K. Burrell, K.C. Gordon, Inorg. Chem. 43 (2004) 2876.
[52] M.J. Frisch, G.W. Trucks, H.B. Schlegel, G.E. Scuseria, M.A. Robb, J.R. Cheeseman, J.A. Montgomery Jr., T. Vreven, K.N. Kudin, J.C. Burant, J.M. Millam, S.S. Iyengar, J. Tomasi, V. Barone, B. Mennucci, M. Cossi, G. Scalmani, N. Rega, G.A. Petersson, H. Nakatsuji, M. Hada, M. Ehara, K. Toyota, R. Fukuda, J. Hasegawa, M. Ishida, T. Nakajima, Y. Honda, O. Kitao, H. Nakai, M. Klene, X. Li, J.E. Knox, H.P. Hratchian, J.B. Cross, C. Adamo, J. Jaramillo, R. Gomperts, R.E. Stratmann, O. Yazyev, A.J. Austin, R. Cammi, C. Pomelli, J.W. Ochterski, P.Y. Ayala, K. Morokuma, G.A. Voth, P. Salvador, J.J. Dannenberg, V.G. Zakrzewski, S. Dapprich, A.D. Daniels, M.C. Strain, O. Farkas, D.K. Malick, A.D. Rabuck, K. Raghavachari, J.B. Foresman, J.V. Ortiz, Q. Cui, A.G. Baboul, S. Clifford, J. Cioslowski, B.B. Stefanov, G. Liu, A. Liashenko, P. Piskorz, I. Komaromi, R.L. Martin, D.J. Fox, T. Keith, M.A. Al-Laham, C.Y. Peng, A. Nanayakkara, M. Challacombe, P.M.W. Gill, B. Johnson, W. Chen, M.W. Wong, C. Gonzalez, J.A. Pople, Gaussian 03, Gaussian, Inc., Pittsburgh, PA, 2003.
[53] J.R. Durig, J. Xiao, J.B. Robb II, F.F.D. Daeyaert, J. Raman Spectrosc. 29 (1998) 463.
[54] T.K. Gounev, G.A. Guirgis, T.A. Mohamed, P. Zhen, J.R. Durig, J. Raman Spectrosc. 30 (1999) 399.
[55] G.A. Guirgis, Y.E. Nashed, J.R. Durig, Spectrochim. Acta A 56 (2000) 1065.
[56] G.A. Guirgis, P. Klaboe, S. Shen, D.L. Powell, A. Gruodis, V. Aleksa, C.J. Nielsen, J. Tao, C. Zheng, J.R. Durig, J. Raman Spectrosc. 34 (2003) 322.
[57] D.A. Long, The Raman Effect: A Unified Treatment of the Theory of Raman Scattering by Molecule, John Wiley & Sons Ltd., London, 2002.
[58] J. Neugebauer, M. Reiher, C. Kind, B.A. Hess, J. Comp. Chem. 23 (2002) 895.
[59] C.M. McGoverin, T.J. Walsh, K.C. Gordon, A.J. Kay, A.D. Woolhouse, Chem. Phys. Lett. 443 (2007) 298.
[60] E. Cances, B. Mennucci, J. Chem. Phys. 114 (2001) 4744.
[61] D.M. Chipman, J. Chem. Phys. 112 (2000) 5558.
[62] D.R. Gamelin, M.W. George, P. Glyn, F.-W. Grevels, F.P.A. Johnson, W. Klotzbuecher, S.L. Morrison, G. Russell, K. Schaffner, J.J. Turner, Inorg. Chem. 33 (1994) 3246.
[63] J. Sherborne, K.C. Gordon, Asian J. Spectrosc. 2 (1998) 137.
[64] J. Sherborne, S.M. Scott, K.C. Gordon, Inorg. Chim. Acta 260 (1997) 199.
[65] S.M. Scott, K.C. Gordon, Inorg. Chim. Acta 254 (1997) 267.
[66] R.J.H. Clark, P.C. Turtle, D.P. Strommen, B. Streusand, J. Kincaid, K. Nakamoto, Inorg. Chem. 16 (1977) 84.
[67] S.M. Scott, A.K. Burrell, P.A. Cocks, K.C. Gordon, J. Chem. Soc. Dalton Trans. (1998) 3679.
[68] R.J.H. Clark, B. Stewart, J. Am. Chem. Soc. 103 (1981) 6593.
[69] C. Manneback, Physica (The Hague) 17 (1951) 1001.
[70] R.W. Nicholls, Astrophys. J. Suppl. Ser. 47 (1981) 279.
[71] K.S. Shin, R.J.H. Clark, J.I. Zink, J. Am. Chem. Soc. 111 (1989) 4244.
[72] J.I. Zink, Coord. Chem. Rev. 64 (1985) 93.
[73] C.S. Yoo, J.I. Zink, Inorg. Chem. 22 (1983) 2474.
[74] Y.Y. Yang, J.I. Zink, J. Am. Chem. Soc. 106 (1984) 1500.
[75] S.K. Doorn, J.T. Hupp, J. Am. Chem. Soc. 111 (1989) 1142.
[76] E.J. Heller, J. Chem. Phys. 62 (1975) 1544.
[77] A.B. Myers, Chem. Rev. 96 (1996) 911.
[78] In the case of [(CN)5Ru-CN-Ru(NH3)5]− this is a rather insightful simplification and is reasonably justified as the normal modes of vibration are in each case dominated by one bond length alteration.
[79] S.K. Doorn, J.T. Hupp, J. Am. Chem. Soc. 111 (1989) 4704.
[80] J. Streiff, J.L. McHale, J. Chem. Phys. 112 (2000) 841.
[81] J.V. Lockard, G. Valverde, D. Neuhauser, J.I. Zink, Y. Luo, M.N. Weaver, S.F. Nelsen, J. Phys. Chem. A 110 (2006) 57.
[82] J.V. Lockard, J.I. Zink, A.E. Konradsson, M.N. Weaver, S.F. Nelsen, J. Am. Chem. Soc. 125 (2003) 13471.
[83] E.A. Plummer, J.I. Zink, Inorg. Chem. 45 (2006) 6556.
[84] U. Fuerholz, S. Joss, H.B. Buergi, A. Ludi, Inorg. Chem. 24 (1985) 943.
[85] W. Leng, F. Wuerthner, A.M. Kelley, J. Phys. Chem. B 108 (2004) 10284.
[86] M.R. Waterland, S.L. Howell, K.C. Gordon, A.K. Burrell, J. Phys. Chem. A 109 (2005) 8826.
[87] D.G. Cuttell, S.-M. Kuang, P.E. Fanwick, D.R. McMillin, R.A. Walton, J. Am. Chem. Soc. 124 (2002) 6.
[88] M.K. Eggleston, D.R. McMillin, K.S. Koenig, A.J. Pallenberg, Inorg. Chem. 36 (1997) 172.
[89] D.R. McMillin, J.R. Kirchhoff, K.V. Goodwin, Coord. Chem. Rev. 64 (1985) 83.
[90] M.R. Waterland, S.L. Howell, K.C. Gordon, J. Phys. Chem. A 111 (2007) 4604.
[91] S.L. Morrison, J.J. Turner, J. Mol. Struct. 317 (1994) 39.
[92] M.W. George, J.J. Turner, Coord. Chem. Rev. 177 (1998) 201.
[93] R.M. Badger, J. Chem. Phys. 3 (1935) 710.
[94] R.M. Badger, J. Chem. Phys. 2 (1934) 128.
[95] S.J. Lind, K.C. Gordon, M.R. Waterland, J. Raman Spectrosc. 39 (2008) 1556.
[96] M.W. Blaskie, D.R. McMillin, Inorg. Chem. 19 (1980) 3519.
[97] L.X. Chen, G.B. Shaw, I. Novozhilova, T. Liu, G. Jennings, K. Attenkofer, G.J. Meyer, P. Coppens, J. Am. Chem. Soc. 125 (2003) 7022.
[98] D.R. Crane, P.C. Ford, J. Am. Chem. Soc. 113 (1991) 8510.
[99] P. Coppens, I.V. Novozhilova, Int. J. Quant. Chem. 101 (2005) 611.
[100] A.Y. Kovalevsky, M. Gembicky, I.V. Novozhilova, P. Coppens, Inorg. Chem. 42 (2003) 8794.
[101] G.B. Shaw, C.D. Grant, H. Shirota, E.W. Castner, G.J. Meyer, L.X. Chen, J. Am. Chem. Soc. 129 (2007) 2147.
[102] M. Iwamura, S. Takeuchi, T. Tahara, J. Am. Chem. Soc. 129 (2007) 5248.
[103] F. Neese, Coord. Chem. Rev. 253 (2009) 526.
[104] Available at http://www.thch.uni-bonn.de/tc/orca/.
[105] T. Petrenko, F. Neese, J. Chem. Phys. 127 (2007) 164319/1.
[106] J. Guthmuller, B. Champagne, J. Chem. Phys. 127 (2007) 164507/1.
[107] T. Petrenko, K. Ray, K.E. Wieghardt, F. Neese, J. Am. Chem. Soc. 128 (2006) 4422.
[108] H.J.A. Jensen, Advances in Quantum Chemistry, Academic Press, Amsterdam, 2005.
[109] A. Mohammed, H. Aagren, P. Norman, Phys. Chem. Chem. Phys. 11 (2009) 4539.
[110] L. Jensen, L.L. Zhao, J. Autschbach, G.C. Schatz, J. Chem. Phys. 123 (2005) 174110/1.
[111] A.J. Esswein, D.G. Nocera, Chem. Rev. 107 (2007) 4022.
[112] H. Ozawa, M. Haga, K. Sakai, J. Am. Chem. Soc. 128 (2006) 4926.

[113] D. Kuang, S. Ito, B. Wenger, C. Klein, J.-E. Moser, R. Humphry-Baker, S.M. Zakeeruddin, M. Graetzel, J. Am. Chem. Soc. 128 (2006) 4146.
[114] G. Ramakrishna, D.A. Jose, K.K. Kumar, A. Das, D.K. Palit, H.N. Ghosh, J. Phys. Chem. B 109 (2005) 15445.
[115] S.E. Koops, B.C. O'Regan, P.R.F. Barnes, J.R. Durrant, J. Am. Chem. Soc. 131 (2009) 4808.
[116] W. Henry, C.G. Coates, C. Brady, K.L. Ronayne, P. Matousek, M. Towrie, S.W. Botchway, A.W. Parker, J.G. Vos, W.R. Browne, J.J. McGarvey, J. Phys. Chem. A 112 (2008) 10704.
[117] J.H. Perng, J.I. Zink, Inorg. Chem. 29 (1990) 1158.
[118] J.J. Turner, M.W. George, F.P.A. Johnson, J.R. Westwell, Coord. Chem. Rev. 125 (1993) 101.
[119] D.C. Grills, J.J. Turner, M.W. George, Compr. Coord. Chem. II 2 (2004) 91.
[120] H.D. Gafney, A.W. Adamson, J. Am. Chem. Soc. 94 (1972) 8238.
[121] E. Borgarello, J. Kiwi, E. Pelizzetti, M. Visca, M. Graetzel, Nature 289 (1981) 158.
[122] C.G. Coates, T.E. Keyes, J.J. McGarvey, H.P. Hughes, J.G. Vos, P.M. Jayaweera, Coord. Chem. Rev. 171 (1998) 323.
[123] M.K. De Armond, M.L. Myrick, Acc. Chem. Res. 22 (1989) 364.
[124] E. Krausz, G. Moran, H. Riesen, Chem. Phys. Lett. 165 (1990) 401.
[125] W.K. Smothers, M.S. Wrighton, J. Am. Chem. Soc. 105 (1983) 1067.
[126] D.J. Liard, M. Busby, P. Matousek, M. Towrie, A. Vlcek Jr., J. Phys. Chem. A 108 (2004) 2363.
[127] Z. Alsindi Wassim, L. Easun Timothy, X.Z. Sun, L. Ronayne Kate, M. Towrie, J.-M. Herrera, W. George Michael, D. Ward Michael, Inorg. Chem. 46 (2007) 3696.
[128] N.H. Damrauer, G. Cerullo, A. Yeh, T.R. Boussie, C.V. Shank, J.K. McCusker, Science 275 (1997) 54.
[129] S. Yoon, P. Kukura, C.M. Stuart, R.A. Mathies, Mol. Phys. 104 (2006) 1275.
[130] A. Cannizzo, F. van Mourik, W. Gawelda, G. Zgrablic, C. Bressler, M. Chergui, Angew. Chem. Int. Ed. 45 (2006) 3174.
[131] A.H.R. Alobaidi, K.C. Gordon, J.J. McGarvey, S.E.J. Bell, J. Grimshaw, J. Phys. Chem. 97 (1993) 10942.
[132] M.R. Waterland, A. Flood, K.C. Gordon, J. Chem. Soc. Dalton Trans. (2000) 121.
[133] K.C. Gordon, J.J. McGarvey, Chem. Phys. Lett. 162 (1989) 117.
[134] C.T. Cunningham, J.J. Moore, K.L.H. Cunningham, P.E. Fanwick, D.R. McMillin, Inorg. Chem. 39 (2000) 3638.
[135] J.J. McGarvey, S.E.J. Bell, K.C. Gordon, Inorg. Chem. 27 (1988) 4003.
[136] W.R. Browne, J.J. McGarvey, Coord. Chem. Rev. 251 (2007) 454.
[137] J.R. Schoonover, C.A. Bignozzi, T.J. Meyer, Coord. Chem. Rev. 165 (1997) 239.